NRC Research Press

ARTICLE

Temporal transferability of LiDAR-based imputation of forest inventory attributes

Patrick A. Fekety, Michael J. Falkowski, and Andrew T. Hudak

Abstract: Forest inventory and planning decisions are frequently informed by LiDAR data. Repeated LiDAR acquisitions offer an opportunity to update forest inventories and potentially improve forest inventory estimates through time. We leveraged repeated LiDAR and ground measures for a study area in northern Idaho, U.S.A., to predict (via imputation) — across both space and time — four forest inventory attributes: aboveground carbon (AGC), basal area (BA), stand density index (SDI), and total stem volume (Vol). Models were independently developed from 2003 and 2009 LiDAR datasets to spatially predict response variables at both times. Annual rates of change were calculated by comparing response variables between the two collections. Additionally, a pooled model was built by combining reference observations from both years to test if imputation can be performed across measurement dates. The R^2 values for the pooled model were 0.87, 0.90, 0.89, and 0.87 for AGC, BA, SDI, and Vol, respectively. Mapping response variables at the landscape level demonstrates that the relationship between field data and LiDAR metrics holds true even though the data were collected in different years. Pooling data across time increases the number of reference observations available to resource managers and may ultimately improve inventory predictions.

Key words: repeated LiDAR acquisitions, imputation, forest inventory, aboveground carbon, change detection.

Résumé : Les décisions concernant la planification et les inventaires forestiers s'appuient souvent sur des données lidar. Les acquisitions lidar récurrentes offrent l'opportunité de mettre à jour les inventaires forestiers et possiblement d'améliorer avec le temps les estimations faites à partir de l'inventaire forestier. Nous avons tiré parti de mesures effectuées sur le terrain et au moyen du lidar dans une aire d'étude du nord de l'Idaho, aux É.-U., pour prédire par imputation, dans l'espace et dans le temps, quatre attributs de l'inventaire forestier) : le carbone aérien (CA), la surface terrière (ST), l'indice de densité du peuplement (IDP) et le volume total de la tige (Vol). Des modèles ont été développés de façon indépendante à partir de données lidar de 2003 et 2009 pour prédire les variables réponse dans l'espace pour chacune des deux années. Les taux annuels de changement ont été calculés en comparant les variables réponse entre les deux ensembles. De plus, un modèle regroupé a été élaboré en combinant les observations de référence des deux années pour vérifier si une imputation pouvait être réalisée à partir des données regroupées des deux années. Les valeurs de R^2 du modèle regroupé étaient, respectivement, 0,87, 0,90, 0,89 et 0,87 pour CA, ST, IDP et Vol. La cartographie des variables réponse à l'échelle du paysage démontre que la relation entre les données terrain et les mesures obtenues grâce au lidar ne change pas même si les données n'ont pas été recueillies durant la même année. Le fait de regrouper les données de plusieurs années augmente le nombre d'observations de référence disponibles pour les gestionnaires des ressources et peut ultimement améliorer les prévisions fondées sur l'inventaire. [Traduit par la Rédaction]

Mots-clés : acquisitions lidar récurrentes, imputation, inventaire forestier, carbone aérien, détection du changement.

Introduction

A detailed forest inventory allows resource managers to make timely and appropriate decisions concerning various management objectives for a forest. Traditionally, continuous forest inventory occurs by measuring permanent sample plots, and inventories are updated through time by remeasurement of plots. Photogrammetry can provide additional information (e.g., species composition), but often the number of attributes obtained is limited and accuracy relies heavily on the skill of the interpreter. Although recent advances in photogrammetry (e.g., photogrammetric matching) has improved the level of detail and accuracy of derived forest inventory data (White et al. 2013*a*; Bohlin et al. 2012), structural information derived from such techniques is still less than what can be derived from light detection and ranging (LiDAR).

Indeed, operational forest inventory and long-term forest planning decisions are also increasingly informed by LiDAR data. LiDAR has been shown to be beneficial for multiple aspects of resource management, including forest inventory (e.g., Næsset 1997; Falkowski et al. 2010), hydrological assessment (e.g., Jones et al. 2008), and forest engineering activities such as road construction (e.g., Aruga et al. 2005), among others. LiDAR collected concurrently with forest inventory field measurements has been used to build predictive models of inventory attributes that can be applied across the LiDAR acquisition extent, ultimately providing landscape to forest-wide estimates of forest inventory attributes (Falkowski et al. 2010). Doing so can be beneficial as ground-based forest inventories across large areas are expensive and time consuming. Although LiDAR acquisitions can also be expensive, efficiencies are gained in terms of reduced field data collection requirements and utility of LiDAR for other applications (Hudak et al. 2009). Hummel et al. (2011) found that the accuracy and cost of performing a LiDAR-based forest inventory are comparable with those associated with a traditional stand-level forest inventory. Accuracies of inventory attributes derived from LiDAR

Received 12 September 2014. Accepted 11 December 2014.

P.A. Fekety and M.J. Falkowski. University of Minnesota, Department of Forest Resources, 1530 Cleveland Ave. N., St. Paul, MN 55108, USA.
A.T. Hudak. U.S. Department of Agriculture, Forest Service, Rocky Mountain Research Station, 1221 S. Main St., Moscow, ID 83843, USA.
Corresponding author: Patrick A. Fekety (e-mail: pafekety@umn.edu).

Published at www.nrcresearchpress.com/cjfr on 16 December 2014.

metrics rival traditional methods, as exemplified by White et al. (2014), who analyzed weight-scaled volumes from 272 harvest stands in Alberta, Canada, and found that LiDAR-based merchantable volume was overestimated by 0.6% compared with using a cover type adjusted volume table, which underestimated volume by 19.8%.

Many studies have used LiDAR metrics to develop models predicting various forest attributes such as basal area (Lefsky et al. 1999), volume (Nilsson 1996), and biomass (for a review, see Zolkos et al. 2013), whereas fewer studies incorporate repeated LiDAR acquisitions into the analysis. Indeed, past research has demonstrated that repeated LiDAR acquisitions provide a temporal component for assessing landscape-level changes (i.e., change detection) and can also be used to estimate height growth (Hopkinson et al. 2007; Yu et al. 2006), monitor changes in tree line position (Næsset and Nelson 2007), and quantify changes in aboveground biomass (Næsset et al. 2013; Hudak et al. 2012).

Statistical imputation has been one method used to support LiDAR-based forest inventory and assessment (Eskelson et al. 2009). In this method, reference observations are imputed (i.e., assigned) to target observations in space (Ohmann and Gregory 2002; Hudak et al. 2008, 2012; Haara et al. 1997). In the context of LiDAR-enhanced forest inventory, usually the target observations are comprised of pixel-level LiDAR metrics derived from a single LiDAR survey. Repeated LiDAR acquisitions provide the opportunity to impute reference observations across time as Nelson et al. (2011) demonstrated with Landsat data. One assumption required is that stand structure conditions sampled at the time of a given LiDAR survey also exist when a subsequent (or previous) LiDAR survey is collected. This is an easy assumption to meet, provided that the range of stand structure conditions represented in the two populations (the study landscape surveyed twice) has not changed significantly. Although stand structure conditions do change locally due to normal forest growth and mortality processes, the range of stand structure conditions should change very little when considering the landscape as a whole. Another assumption is that even though repeated LiDAR acquisitions will undoubtedly be collected with different sensors and using different parameters, the LiDAR metrics will be comparable between acquisitions. Although variation in sensors characteristics between acquisitions can have an impact, binning LiDAR returns to coarser resolutions when calculating metrics (e.g., mean height, canopy cover, etc.) can reduce the sensitivity of forest inventory predictive models to changes in LiDAR acquisition parameters. For example, Hudak et al. (2012) demonstrated that plot-level LiDAR returns between repeated acquisitions had similar spatial distributions despite a 30-fold increase in point density and varying sensor parameters between acquisitions when they were binned to a 20 m × 20 m (400 m²) resolution.

Resource managers could benefit from using LiDAR-based predictive models from past acquisitions to update spatial forest inventories based on more recent acquisitions. In addition to improving historic and contemporary inventory predictions, these new maps of inventory attributes could be used to update forest plans or identify areas of unexpected change across the landscape. Additional potential advantages of repeated LiDAR acquisitions could include (*i*) reducing future forest inventory requirements by identifying undersampled areas and selectively adding additional field inventory plots and (*ii*) applying previous LiDAR-based models to acquisitions from similar forest types that do not have associated field data. Indeed, effective strategies for integrating temporally disparate inventory data via repeated LiDAR acquisitions could greatly reduce future inventory costs and improve the overall accuracy of current, future, and past inventories in the context of retrospective analyses. However, this subject has received little attention in the literature, especially from the perspective of operational forest inventory and assessment.

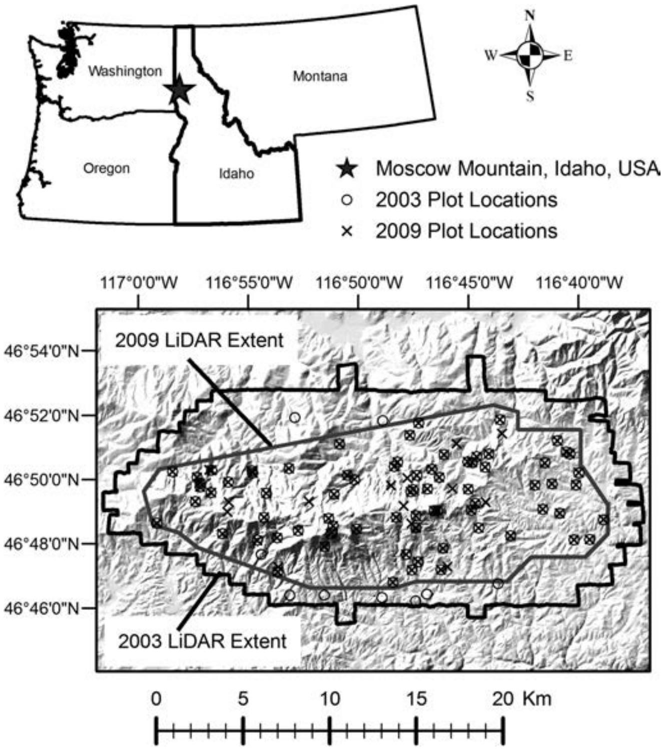

Fig. 1. The Moscow Mountain study area.

The overarching goal of this research was to use repeated field and LiDAR survey data to assess the feasibility of predicting forest inventory attributes across not just space, but also time. In an effort to meet this goal, we addressed the three following hypotheses.

1. Forest inventory attributes can be imputed across space. We developed imputation models using reference observations (i.e., plot-level field and LiDAR data) collected at the same time as the target observations (i.e., gridded LiDAR data).
2. Forest inventory attributes can be imputed across time. We developed imputation models using reference observations collected at different times than the target observations.
3. Forest inventory attributes can be imputed without regard to time. We developed an imputation model using reference observations pooled together without regard to inventory date (i.e., two time periods) and applied it to two sets of target observations collected at different times.

We tested these hypotheses by comparing R^2, mean bias error (MBE), and root mean square distance (RMSD) statistics between measured and imputed values for four forest attributes (aboveground carbon (AGC), basal area (BA), stand density index (SDI), and volume (Vol)) across spatial and temporal domains. We validated the models and applied them spatially to quantify the amount of change between the inventory attributes across the landscape.

Materials and methods

Study area

Moscow Mountain is located in Latah County, Idaho, approximately 13 km northeast of Moscow, Idaho (latitude, 46°48′N; longitude, 116°51′W). The region is a westward extension of the Palouse Mountain Range and is a mixture of ownerships comprised of industrial forests, state forestland, and nonindustrial private forests surrounded by a matrix of agricultural land. The soils are predominately andisols originating primarily from granodirite parent materials with components of volcanic ash and

Table 1. LiDAR acquisition parameters.

	Moscow Mountain 2003	Moscow Mountain 2009
Date	13–14 August 2003	30 June 2009
Acquisition area (ha)	32 708	20 574
Vendor	Horizons, Inc., Rapid City, South Dakota, USA	Watershed Sciences, Inc., Portland, Oregon, USA
LiDAR sensor	Leica ALS 40	Leica ALS 50 Phase II
Laser wavelength (nm)	1 064	1 064
Pulse rate (kHz)	20	up to 150
Scan angle (degrees off nadir)	±18	±14
Altitude (metres above ground level)	2 438	2 000
Footprint diameter (cm)	30	30–45
Return density (points·m^{-2})	0.4	11.95

loess in the upper layers (Soil Survey Staff 2014; U.S. Geological Survey 2006). Elevations range from 776 m to 1517 m above sea level, and the terrain is complex (average slope of 19% and slopes up to 80% across all aspects). Moscow Mountain receives 1115 mm of annual precipitation mostly as snow (annual average 2000–2013; Natural Resources Conservation Service 2014). The mixed conifer forest is comprised of a diversity of tree species. Primary species include ponderosa pine (*Pinus ponderosa* Douglas ex P. Lawson & C. Lawson), Douglas-fir (*Pseudotsuga menziesii* (Mirb.) Franco), grand fir (*Abies grandis* (Douglas ex D. Don) Lindl.), western redcedar (*Thuja plicata* Donn ex D. Don), and western larch (*Larix occidentalis* Nutt.). Secondary species include western white pine (*Pinus monticola* Douglas ex D. Don), lodgepole pine (*Pinus contorta* Douglas ex Loudon), and Engelmann spruce (*Picea engelmannii* Parry ex Engelm.), among others. The primary disturbances for the study area are related to forest management activities, including harvesting, thinning, and prescribed fires.

Field plots

2003 plots

The 2003 field data consists of 84 fixed-area plots (Fig. 1). Plots were allocated across the study area via a stratified random sampling design. The strata included three elevations, three solar insolation levels, and nine canopy cover strata as indicated by a Landsat image derived vegetation index (Pocewicz et al. 2004). Sampling in this manner helped distribute plots across the full range of biophysical characteristics of the study area (Falkowski et al. 2005). Plot centers were geolocated using a Trimble Pro-XR global positioning system (GPS) and differentially corrected using online base station files, resulting in a horizontal accuracy of ±0.8 m and a vertical accuracy of 1.1 m (Hudak et al. 2008). At each plot, all living and standing dead trees with diameter at breast height (DBH) greater than 12.7 cm (5.0 inches (in.)) were measured and tallied in a 0.04 ha (1/10 acre) fixed-area plot.

2009 plots

The 2009 field data consists of 89 fixed-area plots (Fig. 1). The 2009 LiDAR acquisition was smaller in extent than the 2003 collection (Table 1). Seventy-five of the plots measured in 2003 were remeasured in 2009. An updated Landsat image was used to restratify the landscape in 2009. Fourteen field plots were added to fill unrepresented strata to account for changes caused by forest management activities. Although the 2003 plots were not permanently monumented, the 2009 field crew could use a GPS to navigate to the plot center and verify this geolocation using stem map data from the 2003 plot survey. Because the 2009 field crew could not exactly locate the original plot center by such means, new plot centers in 2009 were monumented and regeolocated using differential GPS. Subsequent analysis showed that all 75 repeated plots overlapped to some degree, with a mean offset of 2.67 m and a standard deviation of 1.65 m (Hudak et al. 2012). All living and dead trees with DBH greater than 10.2 cm (4.0 in.) were measured and tallied in the 0.04 ha (1/10 acre) plot. To ensure continuity with the 2003 plot measurements, this study only used trees with DBH greater than 12.7 cm (5.0 in.) when calculating plot-level forest inventory attributes. Additionally, the 2009 field plot measurement protocol required the field crew to identify plots with evidence of harvest activity since the 2003 measurements.

Response variables

Four attributes of interest to ecologists and forest resource managers were chosen as model response variables: AGC, BA, SDI (Reineke 1933), and Vol. AGC was calculated using the Jenkins equations found in the Forest Vegetation Simulator (FVS) Fire Fuels Extension (Reinhardt and Crookston 2003). Living and dead trees were included in the AGC calculation because the LiDAR signal cannot reliably distinguish between living and dead trees in typically closed canopy conditions as exist on Moscow Mountain (Falkowski et al. 2006, 2008). Plot-level BA, SDI, and Vol were calculated by summarizing plot-level tree data using the FVS (Dixon 2014). A summary of plot-level response metrics can be found in Table 2.

LiDAR acquisition and processing

Discrete-return airborne LiDAR data were acquired across Moscow Mountain in 2003 and 2009 (Fig. 1). The 2003 LiDAR acquisition covered all of Moscow Mountain and some surrounding agricultural lands, whereas the 2009 acquisition was constrained to the core area of contiguous forest (Hudak et al. 2012). LiDAR parameters for each collection were similar except for return density, which increased approximately 30-fold as LiDAR sensor technology improved (Table 1). LiDAR returns were classified as either ground or nonground returns using MCC-LiDAR (Evans and Hudak 2007). The MCC-LiDAR algorithm employs thin-plate splines across multiple scales to iteratively classify ground and nonground points based on scale-dependent curvature thresholds. A 1 m spatial resolution digital terrain model (DTM) was generated from each LiDAR acquisition using LiDAR returns classified as ground returns. The DTM from 2003 or 2009 was subtracted from the 2003 or 2009 LiDAR return elevations, respectively, producing normalized LiDAR return heights from which canopy metrics were calculated.

Plot-level LiDAR data were extracted using LAStools (rapidlasso GmbH, Gilching, Germany). The resulting point clouds were processed with FUSION (McGaughey 2012) to calculate plot-level height, strata, cover, and intensity metrics. A 1.37 m (breast height) cutoff was used when calculating LiDAR height metrics. FUSION was also used to calculate the same LiDAR metrics as above, but as a 20 m grid across the study area. For the plot-level LiDAR metrics, a 1.37 m cutoff was used when calculating gridded height metrics.

The 1 m resolution DTMs were resampled to 20 m and used as inputs to the Remote Sensing Application Center's (RSAC; USDA

Table 2. Summary of field data used to build imputatiton models.

Imputation model	Attribute	Minimum	Maximum	Mean	SD
MM03 (n = 84)	AGC (Mg·ha^{-1})	0	380	70	71
	BA (m^2·ha^{-1})	0	100	24	23
	SDI	0	560	174	161
	Vol (m^3·ha^{-1})	0	429	82	88
MM09 (n = 89)	AGC (Mg·ha^{-1})	0	539	70	73
	BA (m^2·ha^{-1})	0	109	24	20
	SDI	0	606	179	143
	Vol (m^3·ha^{-1})	0	544	92	91
MMpooled (n = 165)	AGC (Mg·ha^{-1})	0	539	73	73
	BA (m^2·ha^{-1})	0	109	25	22
	SDI	0	606	184	151
	Vol (m^3·ha^{-1})	0	544	91	90

Note: MM03, Moscow Mountain 2003 model; MM09, Moscow Mountain 2009 model; MMpooled, Moscow Mountain pooled model; SD, standard deviation; AGC, aboveground carbon; BA, basal area; SDI, stand density index; Vol, total stem volume.

Table 3. Potential and final LiDAR metrics used as explanatory variables in the imputation models.

	MM03				MM09				MMpooled			
Explanatory variables	AGC	BA	SDI	Vol	AGC	BA	SDI	Vol	AGC	BA	SDI	Vol
Hmax, height maximum	×	×		×					×	×		×
Hmean, height mean	×	×	×	×	×	×	×	×	×	×	×	×
Hmode, height mode	×	×		×		×	×			×	×	×
Hvar, height variance												
Hskew, height skewness												
Hkurt, height kurtosis												
H05PCT, height 5th percentile	×	×	×	×		×	×			×	×	×
CRR, canopy relief ratio				×		×						
Stratum0, percentage of returns ≤ 0.15 m												
Stratum1, percentage of returns > 0.15 m and ≤ 1.37 m						×	×					
Stratum2, percentage of returns > 1.37 m and ≤ 5 m	×	×		×		×				×	×	
Stratum3, percentage of returns > 5 m and ≤ 10 m										×		
Stratum4, percentage of returns > 10 m and ≤ 20 m	×	×	×	×		×	×		×	×	×	×
Stratum5, percentage of returns > 20 m and ≤ 30 m	×	×	×	×	×	×	×	×	×	×	×	×
Stratum6, percentage of returns > 30 m				×								×
Pct1Rtn_1.37, percentage of first returns > 1.37 m	×	×	×	×	×	×	×	×	×	×	×	×
Pct1Rtn_mode, percentage of first returns above height mode		×				×	×			×	×	
Imean, intensity mean												
Iskew, intensity skewness												
Ikurt, intensities kurtosis												
I05PCT, intensity of 5th percentile												
Elev, DTM elevation	×					×			×	×		×
HEAT, heatload (McCune and Keon 2002)												
Curv, curvature (Zevenbergen and Thorne 1987)												
SCOSA, slope cosine aspect transformation (Evans 2003)												
SSINA, slope sine aspect transformation (Evans 2003)												
TrASP, transformed aspect (Trimble and Weitzman 1956)												
TRIc, topographic roughness index classified (Evans 2004)												
TRIu, topographic roughness index unclassified (Riley et al. 1999)												

Note: MM03, Moscow Mountain 2003 model; MM09, Moscow Mountain 2009 model; MMpooled, Moscow Mountain pooled model; AGC, aboveground carbon; BA, basal area; SDI, stand density index; Vol, total stem volume.

Fig. 2. PCA results demonstrating the extent to which the field measurements encompass landscape structural conditions. Landscape observations with relatively large mean heights are shaded dark red, while observations with relatively low mean heights are shaded light red.

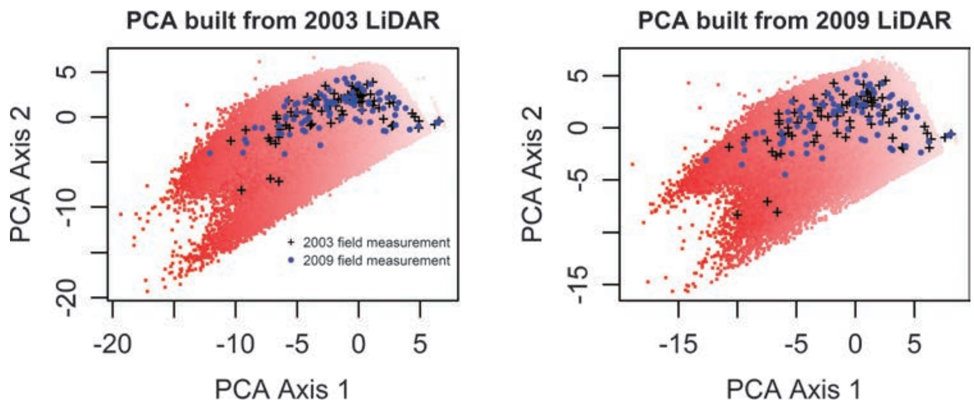

Fig. 3. MM03 model results validated with the 2003 field data. Each field plot is represented by an open circle. The *x* axis represents the value of the nearest neighbor for a specific response variable; the *y* axis represents the plot value summarized by FVS. The shaded region represents the 95% CI. The equation for the line of best fit and corresponding R^2 value are displayed for each plot, along with the mean bias error (MBE) and root mean square difference (RMSD%). AGC, aboveground carbon; BA, basal area; SDI, stand density index; Vol, total stem volume.

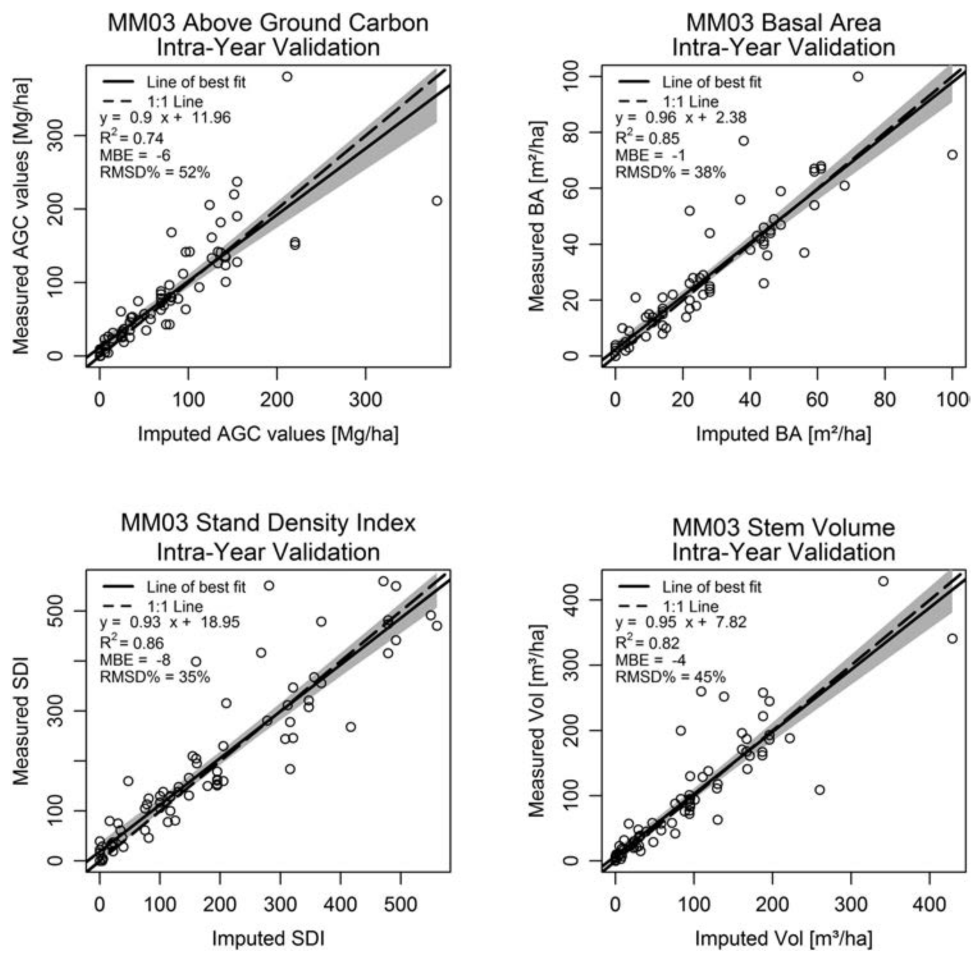

Forest Service, Salt Lake City, Utah) digital elevation model (DEM) toolbox (Ruefenacht 2014), generating wall-to-wall gridded topographic metrics. Plot-level topographic metrics were calculated by extracting area-weighted estimates from output rasters generated by the RSAC DEM toolbox. Plot-level canopy metrics along with topographic metrics and field data were used as reference observations in the imputation models.

Data analysis

Imputation

Random forest (Breiman 2001) imputation models were built using the package yaImpute (Crookston and Finley 2008) of R statistical software (R Core Team 2013). Nearest neighbor (i.e., $k = 1$) imputation was chosen to model the data because multiple re-

Fig. 4. Imputation maps displaying (A) MM03 imputing basal area (BA) from 2003 gridded LiDAR metrics, (B) MM03 imputing BA from 2009 gridded LiDAR metrics, (C) MM09 imputing BA from 2003 gridded LiDAR metrics, and (D) MM09 imputing BA from 2009 gridded LiDAR metrics.

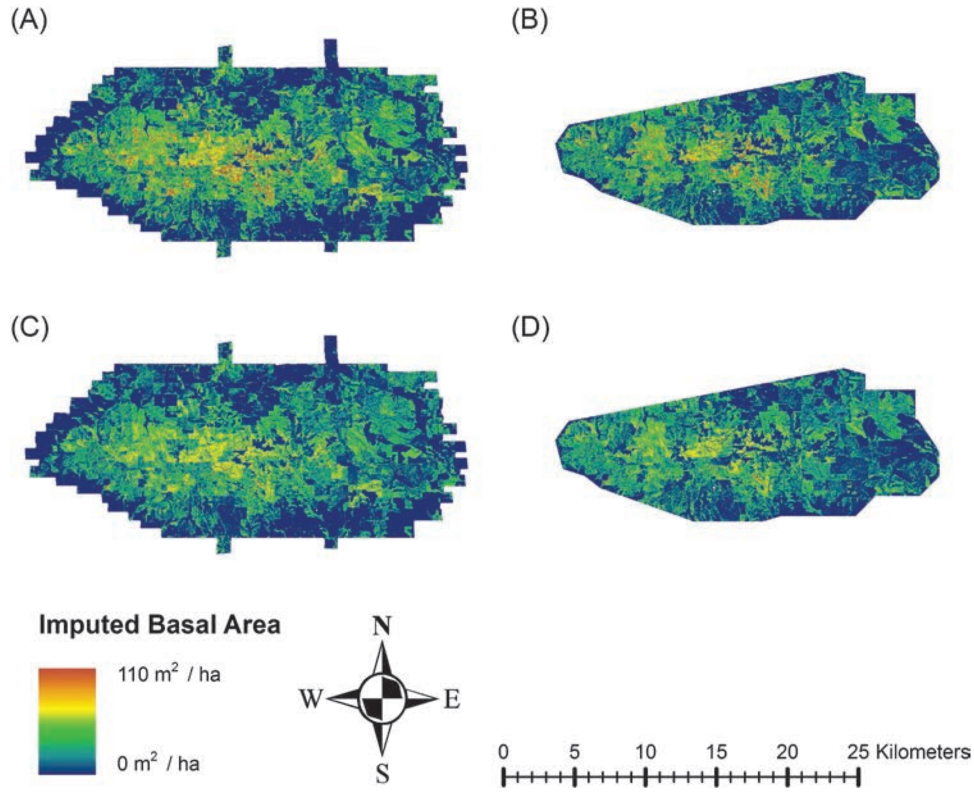

sponses can be simultaneously imputed while preserving the covariance structure of variables derived from the reference observations. The 2003 imputation model for the Moscow Mountain study area (MM03) was derived from the 2003 reference observations, and the independent 2009 imputation model (MM09) was derived from the 2009 reference observations. Additionally, a third imputation model (MMpooled) was derived by pooling the 2003 and 2009 reference observations into a single dataset. Because the spatial extent of the 2003 and 2009 LiDAR collections differed, eight 2003 field plots external to the 2009 LiDAR collection were excluded as reference observations from MMpooled such that the pooled analysis was limited to the area covered by both LiDAR collections (Fig. 1). For all three models, a dataset consisting of 61 explanatory variables was pared down using Gram–Schmidt QR decomposition to remove multicollinear variables (Falkowski et al. 2009; Golub and Van Loan 1996). This resulted in 29 potential explanatory variables for each model (Table 3). A random forest model selection tool based on the model improvement ratio (MIR) was used to select the best suite of predictors for each response variable (Evans and Cushman 2009; Evans et al. 2011; Murphy et al. 2010). The MIR is a scaled value of the random forest prediction error (i.e., percentage increase in mean square error). Through an iterative process, the tool systematically identifies and eliminates the potential predictor variable with the lowest MIR and reruns the random forest algorithm until one predictor variable remains. The final set of predictor variables was identified by the iteration with greatest percentage variation explained. The model selection tool only considers one response variable at a time, and random forest is a nondeterministic algorithm; therefore, the tool was run 100 times for each response variable to ensure stability in the selected model (Table 3).

Sample plot assessment

To determine if the sampling design effectively covered the structural conditions found in the study area, a separate principal component analysis (PCA) was performed on each set of LiDAR metrics (White et al. 2013*b*). Feature spaces spanned by principal components 1 and 2 were plotted. Reference observations from 2003 and 2009 were projected into the feature spaces to assess how well the sampling design covered the structural characteristics found across the study area.

Model assessment

A self-validation process was used to estimate the predictive power of each model by comparing each observed value with the value of its selected nearest neighbor. Also, the dataset not used in training the model was used as an additional validation dataset (i.e., MM03 predictions were validated with the 2009 dataset and vice versa). Maps of the response variables also were imputed across the study area. Comparing nearest neighbor imputed values with the field-measured values allows for intra- and inter-year validation metrics to be calculated. The measured and imputed response variable values were plotted against each other, and a line of best fit was calculated along with associated fit statistics (R^2 and MBE). Ninety-five percent confidence intervals (CI) for the line of best fit were also plotted to determine if the relationship between measured and imputed values was significantly different. The normalized RMSD, RMSD% (eq. 1), which is a validation statistic used with imputation, was computed for each imputation model (Crookston and Finley 2008; Stage and Crookston 2007). RMSD% is calculated as follows:

$$(1) \qquad \mathrm{RMSD\%} = \frac{\sqrt{\frac{1}{n}\sum_{i=1}^{n}(y_i - \hat{y}_i)^2}}{\bar{y}} \times 100$$

where n is the number of samples, y_i and $\hat{y}_i$ are the observed and imputed attributes, respectively, and $\bar{y}$ is the mean of the observed attribute.

Fig. 5. MM09 model results self-validated with the 2009 field data. Each field plot is represented by an open circle. The *x* axis represents the value of the nearest neighbor for a specific response variable; the *y* axis represents the plot value summarized by FVS. The shaded region represents the 95% CI. The equation for the line of best fit and corresponding R^2 value are displayed for each plot, along with the mean bias error (MBE) and root mean square difference (RMSD%). AGC, aboveground carbon; BA, basal area; SDI, stand density index; Vol, total stem volume.

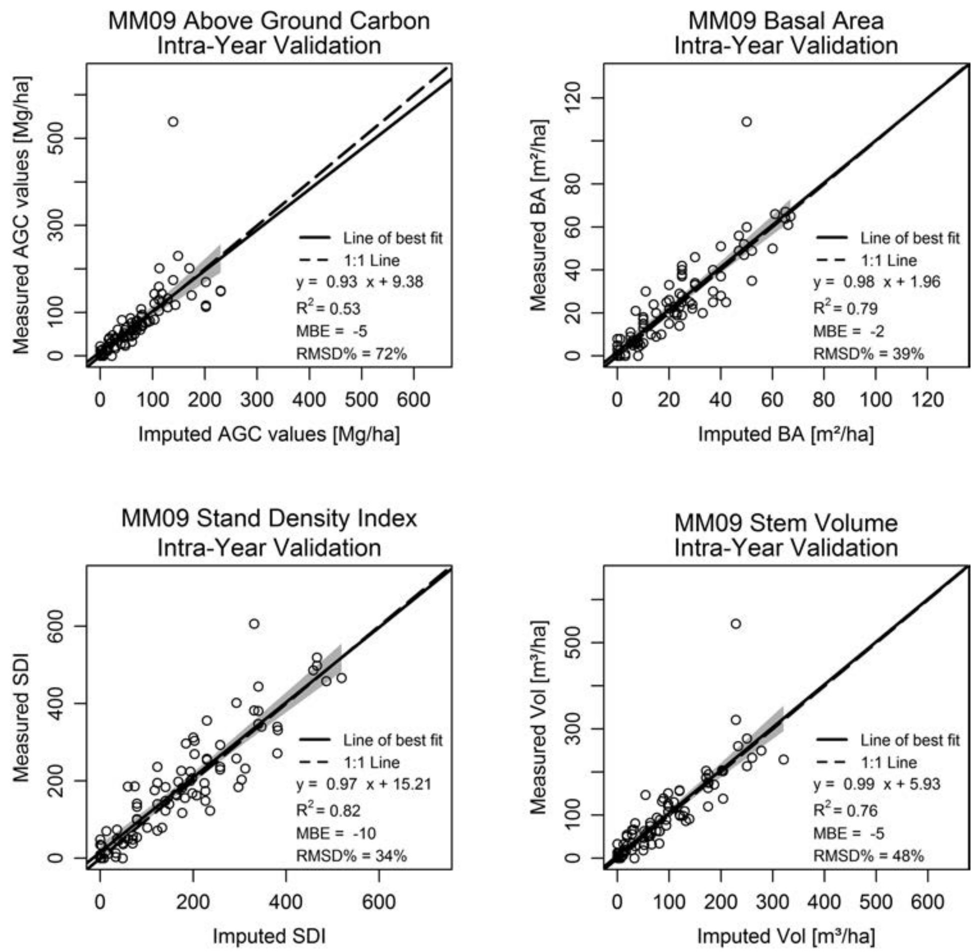

The same metrics described in the intrayear validation section above were calculated for the interyear validation. The 2009 field data were used to validate application of the MM03 imputation model to the 2009 LiDAR, while the 2003 field data were used to validate application of the MM09 imputation model to the 2003 LiDAR. The MM03, MM09, and MMpooled imputation models were also applied to the gridded 2003 and 2009 LiDAR metrics to produce 2003 and 2009 response variable maps of the study area.

Landscape-level trends

Plot-level changes were calculated by subtracting field measurement summaries of 2003 values from field measurement summaries of 2009 values. Landscape-level changes were calculated by comparing response variable maps from the different models. Hudak et al. (2012) found that plots identified as harvested had experienced losses greater than 33 Mg·ha^{-1} AGC (50% of 66 Mg·ha^{-1} of aboveground tree biomass) over the 6-year period; therefore, using this threshold, every pixel was classified as harvested or nonharvested. Pixels that had no LiDAR returns greater than 1.37 m in both 2003 and 2009 were classified as nonforested (Hudak et al. 2012). Landscape-level changes were estimated for harvested, nonharvested, and nonforested areas by subtracting imputation results generated from the 2003 LiDAR collection from imputation results generated from the 2009 LiDAR collection.

Results

Sample plot assessment

PCA analyses were performed to determine if the field plots encompassed the complete range of structural conditions on the landscape. The first four principal components of the PCA built from the 2003 LiDAR metrics explained 66%, 12%, 5%, and 5% of the variation, respectively, and those of the PCA from the 2009 LiDAR metrics explained 60%, 14%, 7%, and 5% of the variation, respectively. Projecting the LiDAR metrics for the 2003 and 2009 field plots into PCA feature space suggests that the stratification scheme based on biophysical characteristics encompassed the majority of the structural conditions across the landscape, although some conditions were not represented. The 2009 field inventory did not capture the full range of variability (e.g., areas with extremely high LiDAR mean heights were not included in the sample); however, these conditions were represented by three field plots in 2003 (Fig. 2). Field data showed that these three plots had two or fewer large trees, and on the landscape level, visual inspection of aerial images showed that the undersampled areas represented stands with few, evenly spaced trees indicative of shelterwood or seed tree harvests. Although the stratification based on biophysical characteristics did not perfectly match the structural conditions, the PCA analysis provides support that the reference observations from 2003 and 2009 can be combined into a

Fig. 6. Imputed and observed response variables when MM03 is applied to the LiDAR metrics calculated within the 2009 field plots. Each field plot is represented by an open circle. The *x* axis represents the value of the nearest neighbor for a specific response variable; the *y* axis represents the plot's value summarized by FVS. The shaded region represents the 95% CI. The equation for the line of best fit and corresponding R^2 value are displayed for each plot, along with the mean bias error (MBE) and root mean square difference (RMSD%). AGC, aboveground carbon; BA, basal area; SDI, stand density index; Vol, total stem volume.

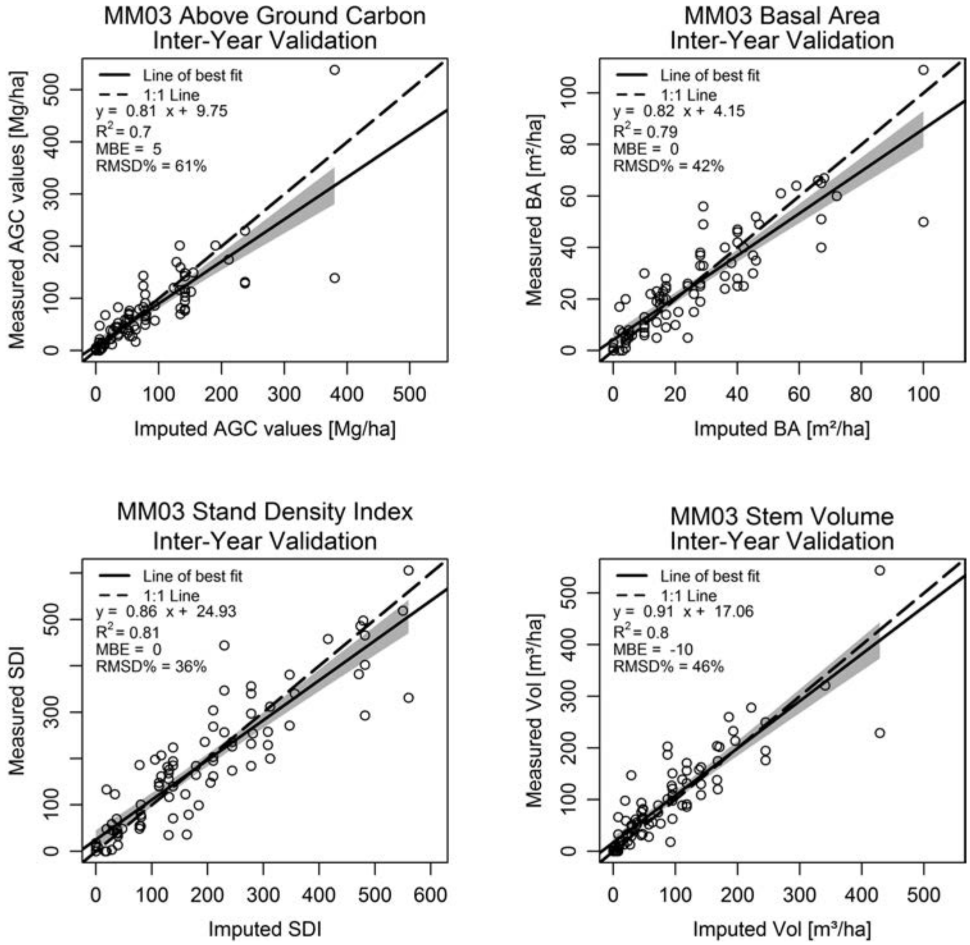

pooled model that ultimately better characterizes the range of variability across the study area.

Fourteen additional field plots were installed in 2009 to account for changes caused by forest management activities that had occurred since 2003. To determine if the additional 14 plots were comparable with the established field plots, Mann–Whitney tests were performed on the forest attributes. In all cases, there was no statistical evidence that the means differed between the established and additional field plots (AGC, $p = 0.373$; BA, $p = 0.283$; SDI, $p = 0.275$; Vol, $p = 0.236$).

Intrayear imputation

The independently derived imputation models, MM03 and MM09, were applied to the target observations (i.e., gridded LiDAR metrics) from 2003 and 2009, respectively, in an effort to confirm the hypothesis that forest inventory attributes can be imputed across space.

Model based on 2003 dataset (MM03)

The MBE suggests that MM03 overpredicts AGC, BA, SDI, and Vol by 6 $Mg \cdot ha^{-1}$, 1 $m^2 \cdot ha^{-1}$, 8 SDI units, and 4 $m^3 \cdot ha^{-1}$, respectively (Fig. 3). Of the four explanatory variables, the slope of the AGC line of best fit showed the greatest deviation from unity (slope = 0.90); additionally, the R^2 value of the line of best fit was the smallest ($R^2 = 0.74$) for AGC. The 95% CI for the line of best fit contains the 1:1 line for BA and Vol; however, at an SDI less than 14 and AGC values less than 35 $Mg \cdot ha^{-1}$, the 95% CI does not contain the 1:1 line (Fig. 3). The RMSD% for AGC, BA, SDI, and Vol were 52%, 38%, 35%, and 45%, respectively. The intrayear imputation map of BA based on MM03 can be found in Fig. 4A; AGC, SDI, and Vol can be found in Supplementary Figs. S1A, S2A, and S3A,[1] respectively.

Model based on 2009 dataset (MM09)

Similar to MM03, the MBE for MM09 overpredicts the four explanatory variables for AGC, BA, SDI, and Vol by 5 $Mg \cdot ha^{-1}$, 2 $m^2 \cdot ha^{-1}$, 10 SDI units, and 5 $m^3 \cdot ha^{-1}$, respectively (Fig. 5). Of the four explanatory variables, the AGC self-validation plot slope also deviated the greatest from unity (slope = 0.93); additionally, the R^2 value was the smallest ($R^2 = 0.53$) for AGC. Unlike the results for MM03, the 1:1 line is within the 95% CI for the line of best fit for the four response variables (Fig. 5). The RMSD% for AGC, BA, SDI, and Vol were 72%, 39%, 34%, and 48%, respectively. The intrayear imputation map of BA based on MM09 can be found in Fig. 4D; AGC, SDI, and Vol can be found in Supplementary Figs. S1D, S2D, and S3D,[1] respectively.

[1]Supplementary data are available with the article through the journal Web site at http://nrcresearchpress.com/doi/suppl/10.1139/cjfr-2014-0405.

Fig. 7. Imputed and observed response variables when MM09 is applied to the LiDAR metrics calculated within the 2003 field plots. Each field plot is represented by an open circle. The *x* axis represents the value of the nearest neighbor for a specific response variable; the *y* axis represents the plot's value summarized by FVS. The shaded region represents the 95% CI. The equation for the line of best fit and corresponding R^2 value are displayed for each plot, along with the mean bias error (MBE) and root mean square difference (RMSD%). AGC, aboveground carbon; BA, basal area; SDI, stand density index; Vol, total stem volume.

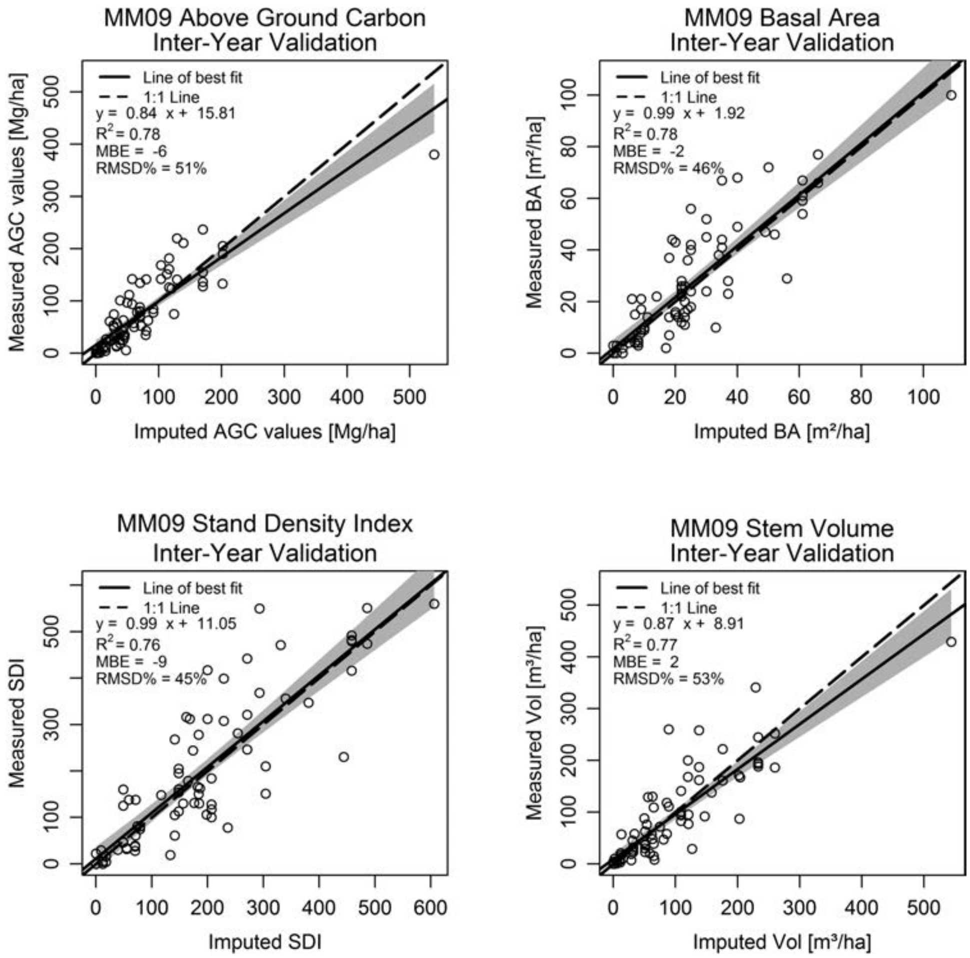

Interyear imputation

We applied the independently derived MM03 and MM09 imputation models to the target observations in 2009 and 2003, respectively, to test the hypothesis that forest inventory attributes can be imputed across time.

MM03 model based predictions from 2009 LiDAR

MBE shows that AGC was underpredicted by 5 $Mg \cdot ha^{-1}$, and Vol was overpredicted by 10 $m^3 \cdot ha^{-1}$; BA and SDI showed practically no bias. The slopes of the line of best fit for interyear validation plots ranged from 0.81 to 0.91, and the four response variables showed portions of the plot that were outside the 95% CI for the line of best fit (Fig. 6). The R^2 value was the smallest and the slope deviated the greatest from unity for AGC. The interyear imputation map of BA based on MM03 can be found in Fig. 4B; AGC, SDI, and Vol can be found in Supplementary Figs. S1B, S2B, and S3B,[1] respectively.

MM09 model based predictions from 2003 LiDAR

MBE shows that MM09 overpredicted AGC by 6 $Mg \cdot ha^{-1}$, BA by 2 $m^2 \cdot ha^{-1}$, and SDI by 9, whereas Vol was underpredicted by 2 $m^3 \cdot ha^{-1}$. Slopes of the line of best fit for the interyear validation plots ranged from 0.84 to 0.99. Portions of the 1:1 line for AGC and Vol were outside the 95% CI for the line of best fit. The 1:1 line is within the 95% CI for the line of best fit for BA and SDI. Once again, the R^2 value was the smallest and the slope deviated the greatest from unity for AGC (Fig. 7). The interyear imputation map of BA based on MM09 can be found in Fig. 4C; AGC, SDI, and Vol can be found in Supplementary Figs. S1C, S2C, and S3C,[1] respectively.

Imputation without regard to time

To test the hypothesis that forest inventory attributes may be imputed without regard to time, the field data from 2003 and 2009 were pooled to create an additional model, MMpooled. As mentioned early, the spatial extent differed between the 2003 and 2009 LiDAR collections and eight field plots scanned by LiDAR only in 2003 were excluded when building MMpooled; six of these eight excluded plots did not have any trees larger than 12.7 cm DBH and the other two excluded plots had low BA (i.e., 5 and 16 $m^2 \cdot ha^{-1}$). MMpooled showed improvement in the fit statistics over MM03 and MM09. For example, the R^2 statistic was 0.90 for MMpooled BA compared with 0.85 and 0.79 for MM03 and MM09 BA, respectively. Additional fit statistics can be found in Fig. 8.

Another way to assess performance of MMpooled was by investigating the proportions of 2003 and 2009 plots chosen as nearest neighbors when imputing at the landscape level. Because 46.1% of the reference observations were measured in 2003 and 53.9% were measured in 2009, we expect nearest neighbors to be assigned to target pixels in the same proportions. Maps of plot identification numbers were generated and analyzed for MMpooled. When using the 2003 LiDAR data as the target observations, the distribu-

Fig. 8. Imputed and observed response variables when MMpooled is applied to the LiDAR metrics calculated within the 2003 and 2009 field plots. The *x* axis represents the value of the nearest neighbor for a specific response variable; the *y* axis represents the plot value summarized by FVS. The solid line is the regression line of best fit, the dashed line is 1:1, and the shaded region represents the 95% CI. The equation for the line of best fit and corresponding R^2 value are displayed for each plot, along with the mean bias error (MBE) and root mean square difference (RMSD%). AGC, aboveground carbon; BA, basal area; SDI, stand density index; Vol, total stem volume.

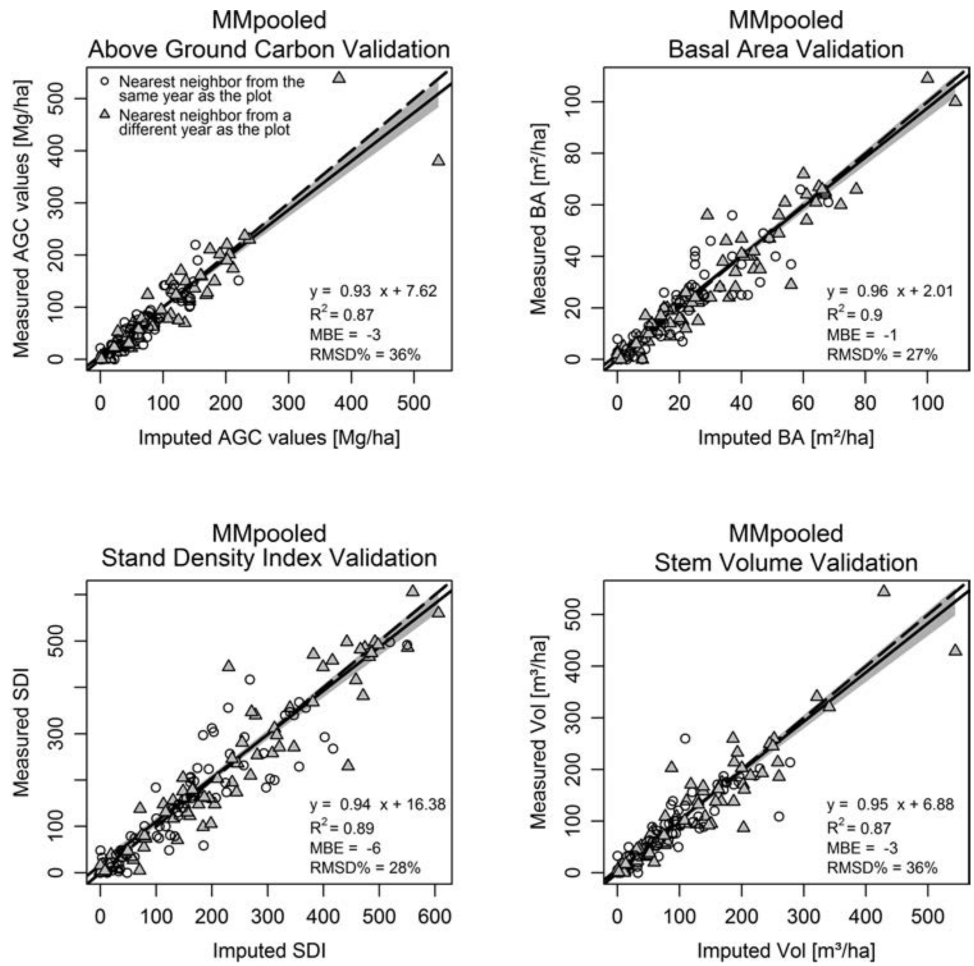

tion of nearest neighbor pixels were 47.3% from 2003 and 52.7% from 2009. When the target observations were the 2009 LiDAR data, MMpooled chose 45.1% and 54.9% of pixels from 2003 and 2009, respectively.

Landscape-level trends

The 2009 field crew identified 20 of the 75 repeated measurement plots (26.7%) as having been harvested sometime between the two measurement periods. Assuming that the lack of monuments on the 55 nonharvested plots with repeated measures had a random and negligible effect on the reference observations, the following plot-level changes were estimated: +1.24 $Mg·ha^{-1}·year^{-1}$ (SE = 0.61 $Mg·ha^{-1}·year^{-1}$) for AGC; +0.35 $m^2·ha^{-1}·year^{-1}$ (SE = 0.15 $m^2·ha^{-1}·year^{-1}$) for BA; +2.96 SDI units$·ha^{-1}·year^{-1}$ (SE = 1.12 SDI units$·ha^{-1}·year^{-1}$) for SDI; and +2.87 $m^3·ha^{-1}·year^{-1}$ (SE = 0.68 $m^3·ha^{-1}·year^{-1}$) for Vol. Plot-level changes of BA are displayed in Fig. 9.

Annual landscape-level changes were calculated in areas classified as harvested, nonharvested, and nonforest (Fig. 10; Table 4). The annual BA growth in nonharvested areas was estimated as follows: +0.46 $m^2·ha^{-1}·year^{-1}$ (SE = 0.0 $m^2·ha^{-1}·year^{-1}$) for MM03; +0.31 $m^2·ha^{-1}·year^{-1}$ (SE = 0.0 $m^2·ha^{-1}·year^{-1}$) for MM09; and +0.38 $m^2·ha^{-1}·year^{-1}$ (SE = 0.0 $m^2·ha^{-1}·year^{-1}$) for MMpooled. Except in three cases, MMpooled produced estimates of change that were either equal to or between the other two models' estimates. The exceptions were as follows: MMpooled estimated less change in volume for harvested areas (MM03, –17.8 $m^3·ha^{-1}·year^{-1}$; MM09, –18.1 $m^3·ha^{-1}·year^{-1}$; MMpooled, –17.4 $m^3·ha^{-1}·year^{-1}$), less change in SDI for all of the study area (MM03, –5.3 $m^3·ha^{-1}·year^{-1}$; MM09, –5.3 $m^3·ha^{-1}·year^{-1}$; MMpooled, –5.2 $m^3·ha^{-1}·year^{-1}$), and less change in Vol for all of the study area (MM03, –2.4 $m^3·ha^{-1}·year^{-1}$; MM09, –2.6 $m^3·ha^{-1}·year^{-1}$; MMpooled, –2.3 $m^3·ha^{-1}·year^{-1}$).

Discussion

An up-to-date forest inventory allows resource managers to make timely decisions, which ultimately supports long-term forest management goals. Forest inventories incorporating LiDAR data provide resource managers with wall-to-wall estimates (i.e., maps) of desired forest attributes for forest planning (White et al. 2013b; Falkowski et al. 2010). When using imputation, combining temporally disparate field plots and associated LiDAR metrics increases the number of reference observations, thus increasing the likelihood that a more similar nearest neighbor will be found, and may ultimately lead to more robust maps of inventory attributes. Imputing across space (termed intrayear imputation in this paper) has been demonstrated by multiple studies (Zald et al. 2014; Hudak et al 2008). Imputing forest attributes across time is novel but not as likely to be applied by resource managers operationally. Imputing forest attributes without regard to time is the novel result of

Fig. 9. Basal area (BA) for plots with repeat measurements (n = 75). The best fit line, linear equation, and R^2 results apply to the nonharvested plots only.

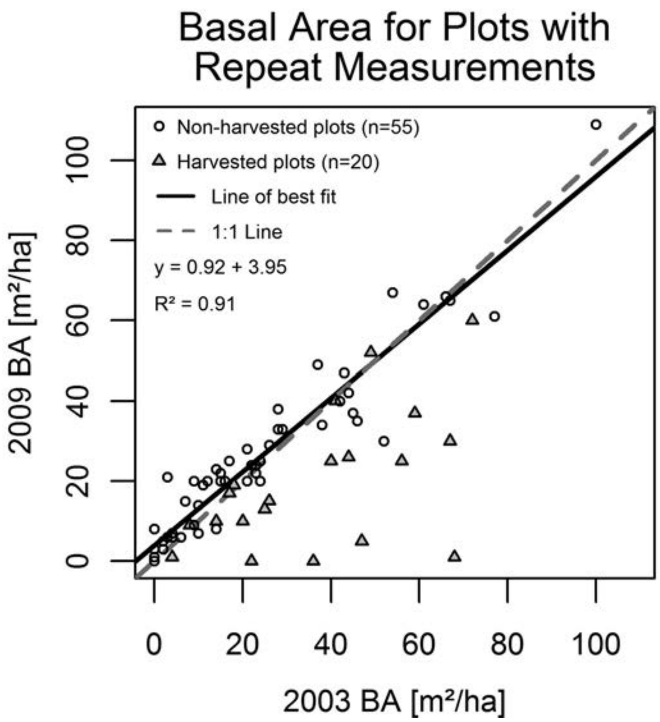

Fig. 10. Maps showing change in aboveground carbon (AGC) for (A) MM03, (B) MM09, and (C) MMpooled.

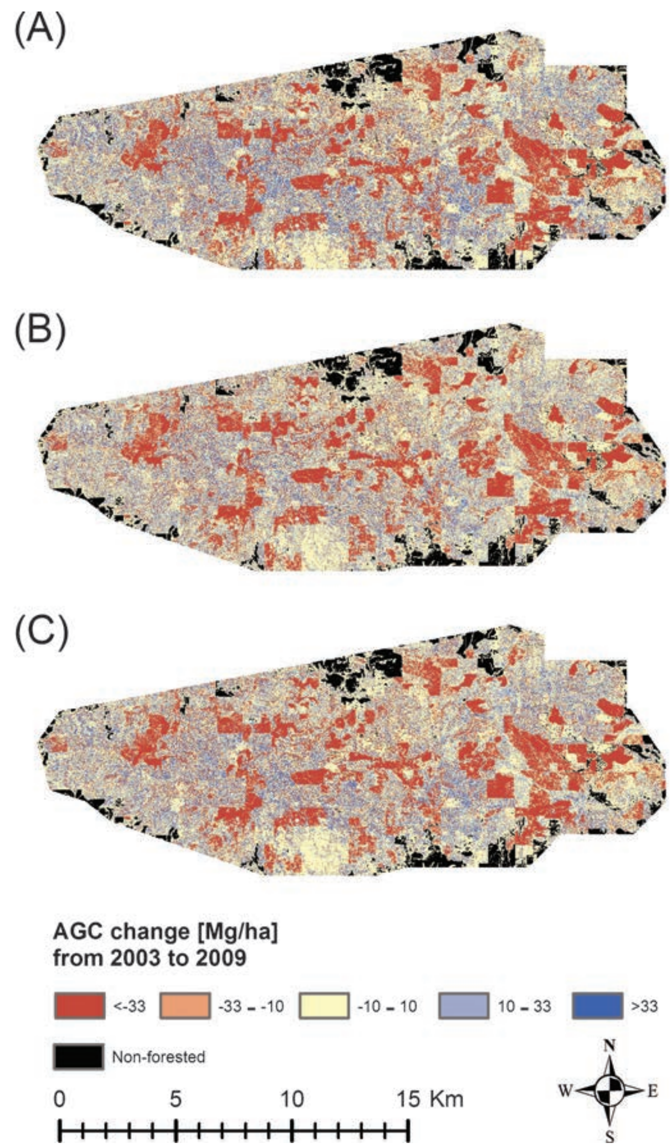

this research and has the most practical implications for forest managers, given the temporally varying and disparate field and LiDAR datasets most often available to them. Therefore, we focus the ensuing discussion on this result, the implications of this result for forest monitoring and change detection, and lastly, point out some important sampling design issues to consider.

Imputation without regard to time

The 2003 and 2009 field sampling designs both effectively sampled a wide variety of forest types present in our study area, ranging from stand regeneration to old single-story and old multistory forests distributed across the landscape. Forest structural conditions can be expected to deviate from their initial landscape distribution over time due to dynamic processes such as forest growth, mortality, and succession. Although the overall spatial distribution of structural conditions changed, we assumed that the structural conditions that existed in 2003 also existed in 2009 somewhere on the landscape. This assumption was supported by the fact that the pooled imputation model had a similar ratio of reference observations from each inventory year to the ratio of nearest neighbor pixels assigned to a given year. In other words, imputing 2003 and 2009 response variables with MMpooled resulted in similar allocations of reference observations from each year. This result demonstrates that imputation across time is possible, but caution is advised when target observations are outside the range of reference observations. For example, it was necessary to limit both the reference observations (sample plots) and target observations (LiDAR collection extents) considered with MMpooled to those observations characterized in both years.

Techniques such as the PCA analysis (White et al. 2013*b*) can provide additional insight into whether or not reference observations from different sampling exercises can be combined. The field plots from 2003 and 2009 are projected to similar areas of the PCA feature spaces regardless of the LiDAR acquisitions. Additionally, three field plots (Fig. 2) from 2003 represented structural conditions not sampled in the 2009 inventory, which ultimately provided an improved set of nearest neighbors in the pooled model.

Identifying landscape-level trends between successive acquisitions

Repeated LiDAR acquisitions are ideal for identifying areas of structural change across a landscape. It is easy to identify stands that experienced a large disturbance (e.g., harvest, stand-replacing fire) by either manual interpretation of maps or automated means, but more difficult to identify subtler disturbances (e.g., single-tree blowdown, pest defoliation). Hudak, et al. (2012) used the same repeated LiDAR and field data employed herein to estimate the change in aboveground tree biomass on Moscow Mountain. Biomass change was estimated for the portion of nonharvested landscape at 4.1 Mg·ha^{-1}·year^{-1}; assuming that 50% of a tree's biomass is carbon, this equates to 2.05 Mg·ha^{-1}·year^{-1}. The current study estimated smaller increases in carbon stocks (Table 4). A key difference between this study and Hudak et al. (2012) is that they did not use a single model to impute across time, but compared aboveground tree biomass between two independently imputed maps. We could not definitively assess which approach is more

Table 4. Estimates of 2003–2009 landscape-level change in harvested, nonharvested, and nonforest areas.

	Land type	MM03	MM09	MMpooled
AGC (Mg·ha^{-1}·year^{-1})	Harvested	–16.2 (0.03)	–14.0 (0.03)	–14.6 (0.03)
	Nonharvested	1.7 (0.01)	1.0 (0.01)	1.3 (0.01)
	Nonforest	0.02 (0.00)	0.01 (0.00)	0.01 (0.00)
	Total	–2.2 (0.01)	–2.0 (0.01)	–2.0 (0.01)
BA (m^2·ha^{-1}·year^{-1})	Harvested	–5.0 (0.01)	–4.7 (0.01)	–4.8 (0.01)
	Nonharvested	0.46 (0.00)	0.31 (0.00)	0.38 (0.00)
	Nonforest	0.00 (0.00)	0.01 (0.00)	0.00 (0.00)
	Total	–0.7 (0.00)	–0.7 (0.00)	–0.7 (0.00)
SDI (SDI units·ha^{-1}·year^{-1})	Harvested	–34.5 (0.07)	–35.2 (0.07)	–34.7 (0.07)
	Nonharvested	2.7 (0.02)	2.1 (0.02)	2.4 (0.02)
	Nonforest	0.04 (0.00)	0.07 (0.00)	0.04 (0.00)
	Total	–5.3 (0.02)	–5.3 (0.02)	–5.2 (0.02)
Vol (m^3·ha^{-1}·year^{-1})	Harvested	–17.8 (0.04)	–18.1 (0.04)	–17.4 (0.04)
	Nonharvested	1.9 (0.01)	1.2 (0.01)	1.6 (0.01)
	Nonforest	0.01 (0.00)	0.01 (0.00)	0.01 (0.00)
	Total	–2.4 (0.01)	–2.6 (0.01)	–2.3 (0.01)

Note: Harvested areas were found by locating pixels that had experienced at least an AGC decrease of 33 Mg·ha^{-1}·year^{-1}. Nonforested areas were identified as having no LiDAR returns above 1.37 m in both 2003 and 2009. All other areas were considered nonharvested. MM03, Moscow Mountain 2003 model; MM09, Moscow Mountain 2009 model; MMpooled, Moscow Mountain pooled model; AGC, aboveground carbon; BA, basal area; SDI, stand density index; Vol, total stem volume.

accurate, but from a practical standpoint, forest managers are less likely to have the luxury of two repeated collections of LiDAR and field data (i.e., Hudak et al. 2012) than a single field survey and two (or more) LiDAR surveys to provide target observations (as tested in this study).

The current study classified 21.1%, 19.6%, and 20.2% of the landscape as harvested based on MM03, MM09, and MMpooled models, respectively, whereas Hudak et al. (2012) estimated 26.3% as harvested. The total landscape-level change for AGC was estimated as –2.2, –2.0, and –2.0 Mg·ha^{-1}·year^{-1} for MM03, MM09, and MMpooled, respectively (Table 4), whereas Hudak et al. (2012) estimated AGC change as –2.85 Mg·ha^{-1}·year^{-1} (–5.7 Mg·ha^{-1}·year^{-1} biomass). Although the estimated changes of AGC within nonharvested areas differ between this study and Hudak et al. (2012), the total landscape-level changes (considering harvested areas as well) are in closer agreement.

It is important to note that an objective of Hudak et al. (2012) was to impute total aboveground biomass, biomass of the dominant species, and the name of the dominant species, whereas the current study imputed AGC, BA, SDI, and Vol. The difference in forest inventory attributes chosen as response variables and the corresponding predictor variables selected as important could also contribute to the lack of agreement between the two studies. As already noted, the summary statistics for AGC were the poorest of the response variables (Figs. 2, 4), which may also contribute to disagreement for this attribute between the two studies.

Inventory design factors impacting results

The forest inventory data in each year were not collected specifically with this study in mind; therefore, minor differences in inventory design exist between the two datasets, impacting the results presented herein. Factors such as total number of plots and the distribution of reference and target observations between sampling years should be carefully considered when developing forest imputation models across time. Each of these variables is considered in more detail in this section.

Number of plots

Installing additional inventory plots provides additional reference observations, which could potentially improve model results by increasing the number of potential nearest neighbors (Stage and Crookston 2007; Moeur and Stage 1995). However, installing additional field plots might be prohibitively expensive or time consuming. Resource managers must balance the cost of performing a forest inventory with the benefit received. As new LiDAR data are collected, managers may opt to not install new field plots for model building and instead impute across time by applying an existing imputation model to the more recent LiDAR data. Alternatively, field plots could be installed to validate the ability of the model to impute across time. In this study, 14 additional field plots were established in 2009 during the landscape restratification. These plots not only filled unrepresented biophysical strata, but also had the advantage of increasing the sample size for MM09 and MMpooled.

Imputing without regard to time would allow managers to use LiDAR and field measures from multiple years to build new models, which effectively increases the number of reference observations used in model building. If plot-level data are to be combined from multiple years, care must be taken to ensure that the plot-level data are summarized consistently. For example, this study excluded trees between 10.2 and 12.6 cm DBH measured in the 2009 field inventory because the minimum DBH in 2003 was 12.7 cm. Likewise, LiDAR metrics need to be calculated using the same equations and parameters if plot-level metrics are going to be combined.

Distribution of observations

It is important that reference observations are well distributed across the full range of forest conditions. Eskelson et al. (2009) noted that target observations representing rare conditions might produce unacceptable nearest neighbor assignments. Indeed, nearest neighbor imputation methods cannot predict outside the range of reference observations (Moeur and Stage 1995). We observed this fact in the current study. The field data used in this study were selected according to a stratified random sampling design in an attempt to capture the complete range of biophysical conditions present in the study area. The PCA analysis highlighted structural conditions that were underrepresented in the 2009 field inventories — shelterwood and seed tree harvests (Fig. 2). Additional field plots in these stands could have improved the model results. However, by pooling the two sets of inventory data, the resulting model better represented the portion of the landscape with high mean heights, suggesting that MMpooled better captured the structural variability on the landscape.

The timing of the 2003 LiDAR collection prevented LiDAR-derived structural metrics from being used in the original landscape stratification; instead, biophysical characteristics were used. Consequently, the field sample only included one plot at the very high end of the structural development gradient present in the study area (i.e., an old-growth plot). This plot had a negative impact on our results because the statistical nearest neighbor to the old-growth plot was quite different in terms of forest structural conditions. Excluding the old-growth plot from this analysis improves the self-validation statistics above those reported here, but because old-growth conditions do exist on the landscape and random forest is a nonparametric technique, the old-growth plot was kept to preserve the overall integrity of inventory maps derived from the imputation. Future studies and application should seriously consider oversampling the tails of the distribution of structural conditions (or other rare conditions) present on the landscape. Doing so would allow the imputation to leverage additional reference observations of rare conditions, especially if characterizing rare conditions is a management priority.

Conclusions

The goal of this study was to investigate imputing forest inventory attributes across time and not just space as a means to enhance inventory accuracy and efficiency. We took advantage of the availability of repeated field and LiDAR surveys to test the feasibility of imputing across time or without regard to time. Models built by pooling reference observations from 2003 and 2009 resulted in nearest neighbors being selected proportional to the number of reference observations used to build the model, regardless of the year in which the plot was measured. This greatly increased the number of plots available to resource managers when building LiDAR-based imputation models. This study demonstrated that the relationship between LiDAR metrics and field data are still valid without regard to time, suggesting that reference observations collected following consistent field sampling and LiDAR processing protocols may be likened to “structural signatures” that can be extended throughout time for imputation modeling and mapping. Landscape-level trends were successfully identified from repeated LiDAR acquisitions, providing resource managers with valuable information regarding temporal changes in forest attributes. Substitution of “space for time” is commonly assumed and applied in ecological studies, but “time for space” substitution may be justifiable as well. These results have practical value to forest resource managers, especially as the number of LiDAR acquisitions across the landscape increases over time.

Acknowledgements

This research was primarily funded by the NASA New Investigator Program via grant NNX14AC26G to Michael Falkowski at the University of Minnesota. We acknowledge additional support from the Agenda 2020 and Big Sky Carbon Sequestration Partnership Programs, Potlatch Forest Holdings, Inc., and Bennett Lumber Products, Inc. for funding LiDAR data collections or processing. We thank the four anonymous reviewers and the Associate Editor for their comments, which improved this article. Finally, we also thank Nicholas Crookston for his assistance with yaImpute.

References

Aruga, K., Sessions, J., and Akay, A.E. 2005. Application of an airborne laser scanner to forest road design with accurate earthwork volumes. J. For. Res. **10**: 113–123. doi:10.1007/s10310-004-0116-9.

Bohlin, J., Wallerman, J., and Fransson, J.E.S. 2012. Forest variable estimation using photogrammetric matching of digital aerial images in combination with a high-resolution DEM. Scand. J. For. Res. **27**(7): 692–699. doi:10.1080/02827581.2012.686625.

Breiman, L. 2001. Random forests. Mach. Learn. **45**(1): 5–32. doi:10.1023/A:1010933404324.

Crookston, N.L., and Finley, A.O. 2008. yaImpute: an R package for kNN imputation. J. Stat. Softw. **23**(10): 1–16. Available from http://www.treesearch.fs.fed.us/pubs/29365.

Dixon, G.E. 2014. Essential FVS: a user's guide to the Forest Vegetation Simulator. USDA Forest Service, Forest Management Services Center, Fort Collins, Colorado. Revised July 2014. Available from http://www.fs.fed.us/fmsc/ftp/fvs/docs/gtr/EssentialFVS.pdf [accessed 10 November 2014].

Eskelson, B.N.I., Temesgen, H., LeMay, V., Barrett, T.M., Crookston, N.L., and Hudak, A.T. 2009. The roles of nearest neighbor methods in imputing missing data in forest inventory and monitoring databases. Scand. J. For. Res. **24**: 235–246. doi:10.1080/02827580902870490.

Evans, J.S. 2003. Topographic radiation index. Environmental Systems Research Institute, Inc., Redlands, California. Available from http://arcscripts.esri.com/details.asp?dbid=12643.

Evans, J.S. 2004. Topographic ruggedness index. Environmental Systems Research Institute, Inc., Redlands, California. Available from http://arcscripts.esri.com/details.asp?dbid=12435.

Evans, J.S., and Cushman, S.A. 2009. Gradient modeling of conifer species using Random Forests. Landsc. Ecol. **5**: 673–683. doi:10.1007/s10980-009-9341-0.

Evans, J.S., and Hudak, A.T. 2007. A multiscale curvature algorithm for classifying discrete return LiDAR in forested environments. IEEE Trans. Geosci. Remote Sens. **45**(4): 1029–1038. doi:10.1109/TGRS.2006.890412.

Evans, J.S., Murphy, M.A., Holden, Z.A., and Cushman, S.A. 2011. Modeling species distribution and change using Random Forest. Chapter 8. *In* Predictive species and habitat modeling in landscape ecology: concepts and applications. *Edited by* C. Ashton Drew, Yolanda F. Wiersma, and Falk Huettmann. Springer, New York. pp. 139–159. doi:10.1007/978-1-4419-7390-0_8..

Falkowski, M.J, Gessler, P.E., Morgan, P., Hudak, A.T., and Smith, A.M.S. 2005. Characterizing and mapping forest fire fuels using ASTER imagery and gradient modeling. For. Ecol. Manage. **217**: 129–146. doi:10.1016/j.foreco.2005.06.013.

Falkowski, M.J., Smith, A.M.S., Hudak, A.T., Gessler, P.E., Vierling, L.A., and Crookston, N.L. 2006. Automated estimation of individual conifer tree height and crown diameter via two-dimensional spatial wavelet analysis of lidar data. Can. J. Remote Sens. **32**: 153–161. doi:10.5589/m06-005.

Falkowski, M.J., Smith, A.M.S., Gessler, P.E., Hudak, A.T., Vierling, L.A., and Evans, J.S. 2008. The influence of conifer forest canopy cover on the accuracy of two individual tree measurement algorithms using LiDAR data. Can. J. Remote Sens. **34**(S2): S338–S350. doi:10.5589/m08-055.

Falkowski, M.J., Evans, J.S., Martinuzzi, S., Gessler, P.E., and Hudak, A.T. 2009. Characterizing forest succession with lidar data: an evaluation for the Inland Northwest, U.S.A. Remote Sens. Environ. **113**: 946–956. doi:10.1016/j.rse.2009.01.003.

Falkowski, M.J., Hudak, A.T., Crookston, N.L., Gessler, P.E., Uebler, E.H., and Smith, A.M.S. 2010. Landscape-scale parameterization of a tree-level forest growth model: a *k*-nearest neighbor imputation approach incorporating LiDAR data. Can. J. For. Res. **40**(2): 184–199. doi:10.1139/X09-183.

Golub, G.H., and Van Loan, C.F. 1996. Matrix computations. 3rd ed. Johns Hopkins University Press, Baltimore, Maryland.

Haara, A., Maltamo, M., and Tokola, T. 1997. The *k*-nearest-neighbour method for estimating basal-area diameter distribution. Scand. J. For. Res. **12**(2): 200–208. doi:10.1080/02827589709355401.

Hopkinson, C., Chasmer, L., and Hall, R.J. 2007. The uncertainty in conifer plantation growth prediction from multi-temporal lidar datasets. Remote Sens. Environ. **112**: 1168–1180. doi:10.1016/j.rse.2007.07.020.

Hudak, A.T., Crookston, N.L, Evans, J.S., Hall, D.E., and Falkowski, M.J. 2008. Nearest neighbor imputation of species-level, plot-scale forest structure attributes from LiDAR data. Remote Sens. Environ. **112**: 2232–2245. doi:10.1016/j.rse.2007.10.009.

Hudak, A.T., Evans, J.S., and Smith, A.M.S. 2009. Review: LiDAR utility for natural resource managers. Remote Sens. **1**(4): 934–951. doi:10.3390/rs1040934.

Hudak, A.T., Strand, E.K., Vierling, L.A., Byrne, J.C., Eitel, J.U.H., Martinuzzi, S., and Falkowski, M.J. 2012. Quantifying aboveground forest carbon pools and fluxes from repeat LiDAR surveys. Remote Sens. Environ. **123**: 25–40. doi:10.1016/j.rse.2012.02.023.

Hummel, S., Hudak, A.T., Uebler, E.H., Falkowski, M.J., and Megown, K.A. 2011. A comparison of accuracy and cost of LiDAR versus stand exam data for landscape management on the Malheur National Forest. J. For. **109**(5): 267–273. Available from http://www.treesearch.fs.fed.us/pubs/38392.

Jones, K.L., Poole, G.C., O'Daniel, S.J., Mertes, L.A.K., and Stanford, J.A. 2008. Surface hydrology of low-relief landscapes: assessing surface water flow impedance using LIDAR-derived digital elevation models. Remote Sens. Environ. **112**: 4148–4158. doi:10.1016/j.rse.2008.01.024.

Lefsky, M.A., Harding, D., Cohen, W.B., Parker, G., and Shugart, H.H. 1999. Surface Lidar remote sensing of basal area and biomass in deciduous forests eastern Maryland, U.S.A. Remote Sens. Environ. **67**(1): 83–98. doi:10.1016/S0034-4257(98)00071-6.

McCune, B., and Keon, D. 2002. Equations for potential annual direct incident radiation and heat load. J. Veg. Sci. **13**: 603–606. doi:10.1111/j.1654-1103.2002.tb02087.x.

McGaughey, R.J. 2012. FUSION/LDV: software for LIDAR data analysis and visualization, version 3.10. USDA Forest Service, Pacific Northwest Research Station, Portland, Oregon. Available from http://forsys.cfr.washington.edu/fusion/FUSION_manual.pdf.

Moeur, M., and Stage, A.R. 1995. Most similar neighbor: an improved sampling inference procedure for natural resource planning. For. Sci. **41**(2): 337–359.

Murphy, M.A., Evans, J.S., and Storfer, A.S. 2010. Quantify *Bufo boreas* connectivity in Yellowstone National Park with landscape genetics. Ecology, **91**: 252–261. doi:10.1890/08-0879.1.

Næsset, E. 1997. Estimating timber volume of forest stands using airborne laser scanner data. Remote Sens. Environ. **61**(2): 246–253. doi:10.1016/S0034-4257(97)00041-2.

Næsset, E., and Nelson, R. 2007. Using airborne laser scanning to monitor tree migration in the boreal–alpine transition zone. Remote Sens. Environ. **110**(3): 357–369. doi:10.1016/j.rse.2007.03.004.

Næsset, E., Bollandsås, O.M., Gobakken, T., Gregoire, T.G., and Ståhl, G. 2013. Model-assisted estimation of change in forest biomass over an 11 year period in a sample survey supported by airborne LiDAR: a case study with post-stratification to provide "activity data". Remote Sens. Environ. **128**: 299–314. doi:10.1016/j.rse.2012.10.008.

Natural Resources Conservation Service (NRCS). 2014. Idaho SNOTEL sites. SNOTEL site no. 989. Available from http://www.wcc.nrcs.usda.gov/nwcc/rgrpt?report=precip_accum_hist&state=ID [accessed 27 February 2015].

Nelson, M.D., Healey, S.P., Moser, W.K., Masek, J.G., and Cohen, W.B. 2011. Consistency of forest presence and biomass predictions modeled across overlapping spatial and temporal extents. Mathematical and Computational Forestry & Natural-Resource Sciences, **3**(2): 102–113. Available from http://mcfns.com/index.php/Journal/article/view/MCFNS.3-102.

Nilsson, M. 1996. Estimation of tree heights and stand volume using an airborne lidar system. Remote Sens. Environ. **56**(1): 1–7. doi:10.1016/0034-4257(95)00224-3.

Ohmann, J.L., and Gregory, M.J. 2002. Predictive mapping of forest composition and structure with direct gradient analysis and nearest-neighbor imputation in coastal Oregon, U.S.A. Can. J. For. Res. **32**(4): 725–741. doi:10.1139/x02-011.

Pocewicz, A.L., Gessler, P., and Robinson, A, P. 2004. The relationship between effective plant area index and Landsat spectral response across elevation, solar insolation, and spatial scales in a northern Idaho forest. Can. J. For. Res. **34**(2): 465–480. doi:10.1139/x03-215.

R Core Team. 2013. R: a language and environment for statistical computing. R Foundation for Statistical Computing, Vienna, Austria. Available from http://www.R-project.org.

Reineke, L.H. 1933. Perfecting a stand-density index for even-aged forests. J. Agric. Res. **46**(7): 627–638.

Reinhardt, E.D., and Crookston, N.L. (*Technical editors*). 2003. The Fire and Fuels Extension to the Forest Vegetation Simulator. USDA Forest Service, Rocky Mountain Research Station, Ogden, Utah, Gen. Tech. Rep. RMRS-GTR-116. Available from http://www.fs.fed.us/fmsc/ftp/fvs/docs/gtr/FFEguide.pdf.

Riley, S.J., DeGloria, S.D., and Elliot, R. 1999. A terrain ruggedness index that quantifies topographic heterogeneity. Intermountain J. Sci. **5**: 23–27.

Ruefenacht, B. 2014. Digital elevation model derivatives. USDA Forest Service, Remote Sensing Applications Center, Salt Lake City, Utah. Available from http://www.fs.fed.us/eng/rsac/ [accessed June 7, 2012].

Soil Survey Staff. 2014. Web soil survey. USDA Natural Resources Conservation Service (NRCS). Available from http://websoilsurvey.nrcs.usda.gov/ [accessed 28 May 2014].

Stage, A.R., and Crookston, N.L. 2007. Partitioning error components for accuracy-assessment of near-neighbor methods of imputation. For. Sci. **53**(1): 62–72. Available from http://www.fs.fed.us/rm/pubs_other/rmrs_2007_stage_a001.pdf.

Trimble, G.R., and Weitzman, S. 1956. Site index studies of upland oaks in the Northern Appalachians. For. Sci. **2**(3): 162–173.

U.S. Geological Survey (USGS). 2006. Preliminary integrated geologic map databases for the United States. Available from http://pubs.usgs.gov/of/2005/1305/#ID [accessed 14 April 2014].

White, J.C., Wulder, M.A., Varhola, A., Vastaranta, M., Coops, N.C., Cook, B.D., Pitt, D., and Woods., M. 2013*a*. The utility of image-based point clouds for forest inventory: a comparison with airborne laser scanning. Forests, **4**: 518–536. doi:10.3390/f4030518.

White, J.C., Wulder, M.A., Varhola, A., Vastaranta, M., Coops, N.C., Cook, B.D., Pitt, D., and Woods., M. 2013*b*. A best practices guide for generating forest inventory attributes from airborne laser scanning data using an area-based approach. Canadian Forest Service, Canadian Wood Fibre Centre Information Report FI-X-010. Available from http://cfs.nrcan.gc.ca/pubwarehouse/pdfs/34887.pdf.

White, J.C., Wulder, M.A., and Buckmaster, G. 2014. Validating estimates of merchantable volume from airborne laser scanning (ALS) data using weight scaled data. For. Chron. **90**(3): 378–385. doi:10.5558/tfc2014-072.

Yu, X., Hyyppä, J., Kukko, A., Maltamo, M., and Kaartinen, H. 2006. Change detection techniques for canopy height growth measurements using airborne laser scanner data. Photogramm. Eng. Remote Sensing, **72**(12): 1339–1348. doi:10.14358/PERS.72.12.1339.

Zald, H.S.J, Ohmann, J.L., Roberts, H.M., Gregory, M.J., Henderson, E.B., McGaughey, R.J., and Braaten, J. 2014. Influence of lidar, Landsat imagery, disturbance history, plot location accuracy, and plot size on accuracy of imputation maps of forest composition and structure. Remote Sens. Environ. **143**: 26–38. doi:10.1016/j.rse.2013.12.013.

Zevenbergen, L.W., and Thorne, C.R. 1987. Quantitative analysis of land surface topography. Earth Surf. Processes Landforms, **12**: 47–56. doi:10.1002/esp.3290120107.

Zolkos, S.G., Goetz, S.J., and Dubayah, R. 2013. A meta-analysis of terrestrial aboveground biomass estimation using lidar remote sensing. Remote Sens. Environ. **128**: 289–298. doi:10.1016/j.rse.2012.10.017.